JPE 18-4-13

https://doi.org/10.6113/JPE.2018.18.4.1086
ISSN(Print): 1598-2092 / ISSN(Online): 2093-4718

Filterless and Sensorless Commutation Method for BLDC Motors

Shahin Mahdiyoun Rad* and Mohammad Reza Azizian†

†,*Department of Electrical Engineering, Sahand University of Technology, Tabriz, Iran

Abstract

This study presents a new sensorless commutation method for brushless direct current motors to replace Hall sensor signals with virtual Hall signals. The importance of the proposed method lies in the simultaneous elimination of the phase shifter and the low-pass filters, which makes the method simple and cost-effective. The method removes high ripple switching noises from motor terminals, thereby decreasing motor losses. The proposed method utilizes unfiltered line voltages with notches caused by current commutation. Hence, specific sign signals are defined to compensate for the effects of commutation noise. The proposed method is free from phase delay that originates from low-pass filters. The method directly produces virtual Hall signals, and thus, it can be interfaced with low-cost commercial commutation integrated circuits based on Hall sensors. Simulation and experimental results show the effectiveness and validity of the proposed method.

Key words: Brushless DC motor, Current commutation, Filterless, Rotor position detection, Sensorless

I. INTRODUCTION

Brushless direct current (BLDC) motors are extensively used in the industry due to their advantages, which include high efficiency, low maintenance, light weight, good controllability over a wide range of speed and compact structure [1]-[3]. BLDC motors require rotor position information to properly perform current commutation in stator windings. In general, rotor position is detected by Hall sensors placed within a motor. These position sensors complicate system configuration and increase motor cost and size. In addition, these sensors can reduce system reliability because sensor failure may cause control system instability. Furthermore, the operation of BLDC motors is limited because of the sensitivity of Hall sensors to noise, temperature, and mechanical vibrations [4]-[6]. To overcome these disadvantages, sensorless commutation methods have received considerable attention.

The first sensorless commutation method for BLDC motors was introduced in [7]. In this method, commutation is performed via the zero-crossing detection of back electromotive force (EMF) and 30 electrical degrees phase shift. In the aforementioned method, the terminal voltage of the inactive phase is monitored relative to the virtual neutral point. This back-EMF sensing technique requires a virtual neutral point. Moreover, the measured neutral point voltage and the terminal voltages include high-frequency ripples due to the pulse-width modulation (PWM) switching of the inverter. Therefore, the conventional sensorless method requires low-pass filters (LPFs) to eliminate switching noises. The main problem in the use of LPFs is that it causes speed-dependent phase delay and position error, particularly at high speeds. Consequently, this approach limits the high-speed operation capability of BLDC motors because the phase delay of the estimated position signal causes the misalignment of the phase current with the rotor position. Therefore, torque ripples occur, which reduce the average torque and motor efficiency [8]. Furthermore, the detected zero-crossing points (ZCPs) inherently lead the actual commutation points (CPs) by 30° in this method. Hence, a phase shifter is required to determine the appropriate CPs. Phase-shifting makes the sensorless commutation process complicated because it requires an expensive digital signal processor (DSP). Studies that have been conducted to improve the traditional back-EMF-based sensorless method can be classified into two groups: 1) studies that have eliminated only LPFs [9]-[15], and 2) studies that have removed only phase shifters [16]-[19].

Manuscript received Aug. 11, 2017; accepted Mar. 13, 2018
Recommended for publication by Associate Editor Kwang-Woon Lee.
†Corresponding Author: azizian@sut.ac.ir
Tel: +98-41-33459352, Fax: +98-41-33454322, Sahand Univ. Tech.
*Dept. of Electrical Engineering, Sahand University of Technology, Iran

The first group of studies has focused on eliminating LPFs. In [9], the PWM signal is applied only to upper switches, and the terminal voltage of the unexcited phase is sampled only during PWM off time. The disadvantage of this approach is that it requires minimum PWM off time to properly sample the terminal voltage, which limits the duty cycle and yields incomplete use of the direct current (DC) voltage source. Moreover, this approach is unsuitable at high speeds when PWM off time is extremely short. To solve this problem, a complementary method is introduced in [10]. This method samples terminal voltages during either PWM on time or off time. In [11]-[13], CPs are extracted by detecting and then 30° shifting the ZCPs of the line voltage differences sampled during PWM on time. In [14], a Z-source inverter was utilized to supply the BLDC motor, and the unexcited phase voltage was sampled in the shoot-through vectors. Although the methods presented in [9]-[14] do not need an LPF, they require a phase shifter and a special PWM switching scheme to correctly sample motor voltages. In [15], a digital filtering procedure was applied to the unfiltered terminal voltages relative to the neutral point. Although this method eliminated LPFs, it is complicated and requires a phase shifter and a neutral point voltage.

In the second group of studies, the phase shifter has been eliminated, but the phase delay resulting from LPFs has not been considered and discussed. In [16], it is shown that the ZCPs of the line back-EMFs coincide with the actual CPs, and thus, the phase shifter can be eliminated. Furthermore, the line voltages contain the corresponding line back-EMFs. Consequently, filtered line voltages are used instead of line back-EMFs in [16]-[19]. However, phase delay is inevitable because LPFs are used to eliminate switching and commutation noises. In [19], phase delay caused by LPFs was nearly compensated for but only at the nominal speed of the motor by adjusting the hysteresis band of the comparators. Hence, this approach is inappropriate for variable speed drives.

In [20], [21], specific methods based on $90-\alpha$ or $150-\alpha$ phase shifting were presented. In these methods, the ZCPs of heavily filtered motor voltages are used to determine CPs. In addition to their complexity, these methods require variable phase shifting because the total phase delay varies with motor speed. Line voltages were also used in [22]. However, the developed method is more complicated and requires two-step filtering and neutral point voltage. The methods proposed in [23]-[25] determined CPs based on the ZCPs of the specific error functions obtained from the filtered voltages of a four-switch drive. Although the phase shifter is eliminated, the phase delay that originates from LPFs deteriorates motor performance.

To overcome the aforementioned drawbacks, the method proposed in the current study simultaneously eliminates LPFs and the phase shifter. Accordingly, unfiltered line voltages are used and new sign signals are defined and introduced to compensate for the commutation ripple effects. Virtual Hall signals (VHSs) are estimated by applying a set of proposed logical operations to the defined sign signals. The method can be easily implemented using simple circuits without requiring high-cost DSP. Furthermore, the VHSs obtained from the method are free from phase delay because no LPF is used. Hence, the proposed method can be utilized at a wide range of speed.

The remainder of the paper is organized as follows. Section II investigates the effect of current commutation on motor voltage. The proposed method for generating compensator signals and extracting VHSs is presented in Section III. The simulation and experimental results are provided in Sections IV and V, respectively, to verify the effectiveness of the proposed sensorless commutation method. Finally, the conclusions of the study are summarized in Section VI.

II. Current Commutation Effects on Line Voltages

In general, the PWM method is used to control BLDC motors. For a high-speed BLDC motor, the PWM method produces large high-frequency ripples in the current, which will inevitably increase copper and rotor iron losses [20]-[22], [26]-[30]. Furthermore, the variable DC-link inverter can provide a more stable performance for the sensorless control of a BLDC motor than the PWM method at high speeds [31]. Fig. 1 shows the equivalent circuit of a three-phase Y-connected BLDC motor that is fed by a full-bridge inverter. A buck converter is used in front of the three-phase inverter to regulate the DC-link voltage via the duty cycle of switch S_7 as follows:

$$V_{dc} = DV_{in} \tag{1}$$

where V_{dc} is the DC-link voltage, V_{in} is the buck converter input voltage, and D is the duty cycle of converter switch S_7.

The voltage equations of the BLDC motor shown in Fig. 1 are given as

$$\begin{pmatrix} V_{ag} \\ V_{bg} \\ V_{cg} \end{pmatrix} = R \begin{pmatrix} i_a \\ i_b \\ i_c \end{pmatrix} + L \frac{\mathrm{d}}{\mathrm{dt}} \begin{pmatrix} i_a \\ i_b \\ i_c \end{pmatrix} + \begin{pmatrix} e_a \\ e_b \\ e_c \end{pmatrix} + \begin{pmatrix} V_{Ng} \\ V_{Ng} \\ V_{Ng} \end{pmatrix} \tag{2}$$

where V_{ag}, V_{bg}, and V_{cg} are the motor terminal voltages with respect to the DC-link ground g. The stator phase currents are indicated by i_a, i_b, and i_c. Stator resistance, stator inductance, and motor neutral point voltage relative to the ground g are denoted by R, L, and V_{Ng}, respectively. The trapezoidal back-EMF voltages of the BLDC motor indicated by e_a, e_b, and e_c are defined as

$$\begin{aligned} e_a &= K_e \omega_m F(\theta_e) \\ e_b &= K_e \omega_m F(\theta_e - 2\pi/3) \\ e_c &= K_e \omega_m F(\theta_e + 2\pi/3) \end{aligned} \tag{3}$$

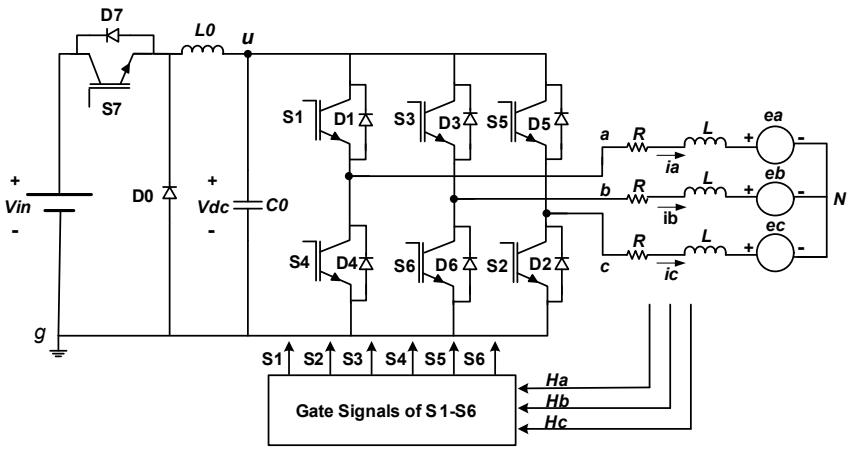

Fig. 1. Equivalent circuit of the Y-connected BLDC motor and its inverter topology based on the buck converter.

where K_e, ω_m, and θ_e are the motor voltage constant, angular velocity, and electrical position of the rotor, respectively. F represents the trapezoidal function and can be expressed as

$$F(\theta_e)=\begin{cases}(6/\pi)\theta_e & 0\le\theta_e\le\pi/6\\ 1 & \pi/6\le\theta_e\le5\pi/6\\ 1-(6/\pi)(\theta_e-5\pi/6) & 5\pi/6\le\theta_e\le7\pi/6\\ -1 & 7\pi/6\le\theta_e\le11\pi/6\\ -1+(6/\pi)(\theta_e-11\pi/6) & 11\pi/6\le\theta_e\le2\pi\end{cases} \quad (4)$$

Fig. 2 shows the phase currents, trapezoidal back-EMF voltages, electromagnetic torque, and ideal Hall signals (IHSs) of the BLDC motor in an ideal case. For the normal operation of a BLDC motor, its phase currents and back-EMFs should be aligned to produce smooth and ripple-free torque, as shown in Fig. 2. Otherwise, the efficiency of the motor will decrease. Therefore, rotor position identification is of particular importance in the sensorless commutation of BLDC motors.

As mentioned earlier, CPs can be obtained without a phase shifter by detecting the ZCPs of filtered line voltages. However, LPFs cause the estimated commutation signals to lag behind IHSs. To eliminate the speed-dependent phase delay resulting from LPFs, unfiltered line voltages are used in the present work. In this regard, switches S_1 to S_6 in Fig. 1 are turned on and off only when they perform current commutation. Therefore, motor terminal voltages do not have undesirable high-frequency PWM switching noise, and consequently, no LPF is required. We define a set of sign signals for line voltages as follows:

$$\begin{aligned}D_{ac}&=(1+\text{sign}(V_{ag}-V_{cg}))/2\\ D_{ba}&=(1+\text{sign}(V_{bg}-V_{ag}))/2\\ D_{cb}&=(1+\text{sign}(V_{cg}-V_{bg}))/2\end{aligned} \quad (5)$$

where all the voltages are unfiltered. Fig. 3 shows the unfiltered line voltage V_{ac}, its sign signal, and IHS. The ripples due to current commutation appear in unfiltered line voltages.

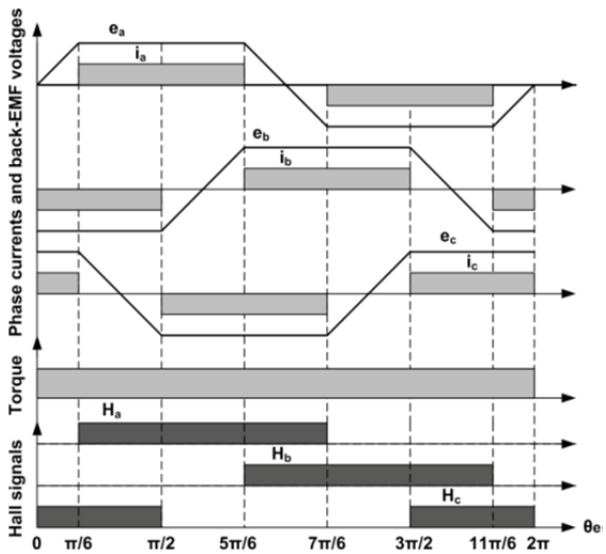

Fig. 2. Phase currents, trapezoidal back-EMF voltages, electromagnetic torque, and Hall signals of a BLDC motor in an ideal case.

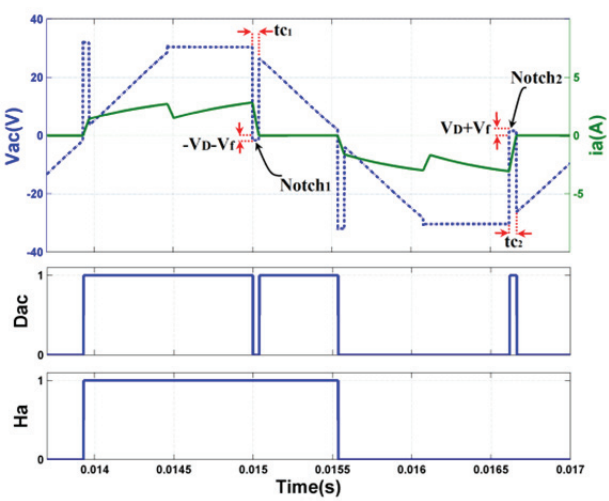

Fig. 3. From top to bottom: unfiltered line voltage V_{ac}, phase current, sign signal of V_{ac}, and IHS for phase "a".

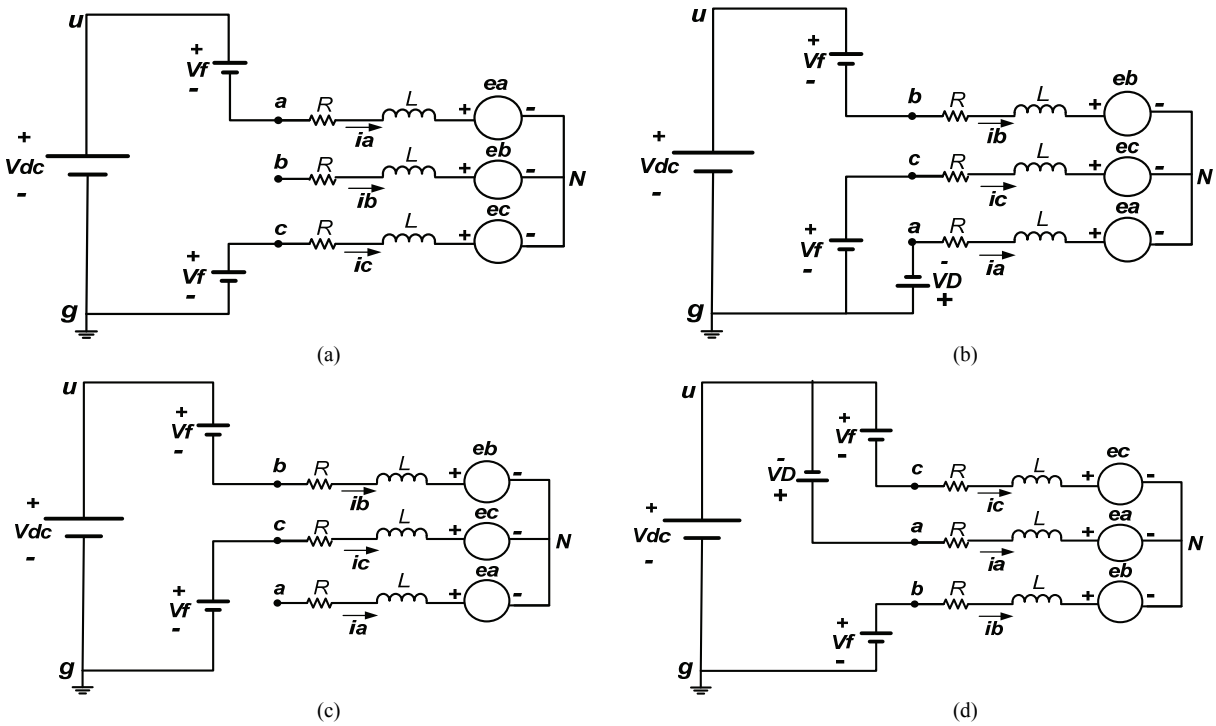

Fig. 4. Equivalent circuit of the motor and its inverter: (a) Before the first notch, (b) During the first notch, (c) After the first notch, (d) During the second notch.

Therefore, the sign signal obtained from the unfiltered line voltage differs from the IHS.

Two notches are found in the line voltage waveform. These notches cross the zero axis and cause zero-crossing errors. We consider the first notch that appears in the positive half cycle of V_{ac}. Before the first notch, switches S_1 and S_2 are on; thus, phases "*a*" and "*c*" are conducting. The equivalent circuit is shown in Fig. 4(a). The voltage and current equations can be expressed as

$$\begin{aligned} V_{ac} &= V_{dc} - 2V_f \\ i_a &= -i_c = I \ \ and \ \ i_b = 0 \end{aligned} \tag{6}$$

where V_f denotes transistor forward voltage drop. Voltage V_{ac} indicates a positive value during this interval. At the end of this interval, switch S_1 turns off and switch S_3 turns on. This situation transfers the current from phase "*a*" to phase "*b*". The current of phase "*a*" does not immediately decrease to zero due to the inductance of the stator windings. Hence, diode D_4 conducts until i_a becomes zero. The equivalent circuit during this period is shown in Fig. 4(b). Current commutation causes the voltage V_{ac} to change from the previous positive value of $V_{dc} - 2V_f$ to the negative value of $-V_D - V_f$ (V_D denotes diode forward voltage drop).

When the Kirchhoff current law is applied to the neutral point N and the Kirchhoff voltage law is applied to the inner loops of the equivalent circuit, the voltage and current equations can be written as

$$\begin{aligned} &-V_{dc} + V_f + R\,i_b + L\frac{di_b}{dt} + e_b - e_c - L\frac{di_c}{dt} - Ri_c + V_f = 0 \\ &-V_f + Ri_c + L\frac{di_c}{dt} + e_c - e_a - L\frac{di_a}{dt} - Ri_a - V_D = 0 \\ &i_a + i_b + i_c = 0 \end{aligned} \tag{7}$$

The current of phase "*a*" is derived as follows by solving Eq. (7):

$$i_a(t) = I\,e^{-\frac{t}{\tau}} + \frac{1}{3R}(V_{dc} + 2V_D + 2e_a - e_c - e_b)(1 - e^{-\frac{t}{\tau}}) \tag{8}$$

where $\tau = \frac{L}{R}$ is the time constant, and I is the motor phase current prior to starting the current commutation process. When the current of phase "a" becomes zero, current commutation is completed and commutation duration can be calculated as

$$t_{c1} = -\frac{L}{R} Ln\left(\frac{1}{1 + 3RI/(V_{dc} + 2V_D + 2e_a - e_b - e_c)}\right) \tag{9}$$

At the end of the commutation period, diode D_4 turns off and the equivalent circuit is shown in Fig. 4(c). The amplitude of voltage V_{ac} immediately after the end of the current commutation can be approximately obtained as

$$V_{ac} = e_a - e_c - L\frac{di_c}{dt} - Ri_c \approx 2K_e\omega_m - L\frac{di_c}{dt} - Ri_c >> 0. \tag{10}$$

The current of phase "*c*" is negative in this interval according to the equivalent circuit shown in Fig. 4(c). Hence,

the voltage V_{ac} expressed in Eq. (10) indicates a positive value and is changed compared with the previous negative value of $-V_D - V_f$.

To date, we have analyzed the commutation of the positive current from phase "*a*" to phase "*b*". We then consider the negative half cycle of line voltage V_{ac} , in which the negative current transfers from phase "*a*" to phase "*b*". The second notch can be studied by adopting the same procedure. The equivalent circuit of the motor and inverter during this commutation interval is shown in Fig. 4(d). The value of line voltage V_{ac} is obtained as $V_D + V_f$, which confirms that the polarity of the line voltage has changed. Thus, current commutation unfavorably alters the polarity of line voltage V_{ac} twice a cycle and makes its sign signal unsuitable for sensorless commutation. The motor is symmetrical, and thus, the same process is applied to the other two unfiltered line voltages, namely, V_{cb} and V_{ba}.

III. Proposed Method for Determining VHSs

The unfiltered voltages (V_{cg} and V_{ag}) and the line voltage (V_{ac}), which is generated by subtracting V_{cg} from V_{ag} , are shown in Fig. 5. The notches of V_{ag} coincide with those of the line voltage that cross zero. Hence, we investigate V_{ag} for extracting compensator signals. We consider the waveform of V_{ag} shown in Fig. 5. In Section 1, the upper switch of the phase "*a*" (S_1) is turned on (Fig. 4(a)). Hence, the amplitude of V_{ag} is $V_{dc} - V_f$. In Section 2, the current commutates from phase "*a*" to phase "*b*" and the lower freewheeling diode of phase "*a*" (D_4) is conducting (Fig. 4(b)). Therefore, the amplitude of V_{ag} is $-V_D$. In Section 3, phase "*a*" is floating (Fig. 4(c)). In Section 4, the lower switch of phase "*a*" (S_4) is turned on and the amplitude of V_{ag} is V_f . In Section 5, the current is commutating from phase "*a*" to phase "*b*" and the upper freewheeling diode of phase "*a*" (D_1) is conducting (Fig. 4(d)). Thus, the value of V_{ag} is $V_{dc}+V_D$. The value of V_{ag} is negative only when diode D_4 is conducting, i.e., in Section 2, which coincides with the first notch of V_{ac} . Hence, we can use the sign signal of V_{ag} to compensate for the first notch of V_{ac} . In Sections 2 and 4, however, the amplitude of V_{ag} is extremely small compared with the maximum voltage value. Therefore, when we rescale voltage V_{ag} for a low-voltage control circuit, its magnitude becomes extremely small in the aforementioned sections. Consequently, its detection will be difficult. To address this problem, an efficient sensing circuit is proposed, as shown in Fig. 6(a). Diode D_1' causes the circuit to have two different rescaling ratios as follows:

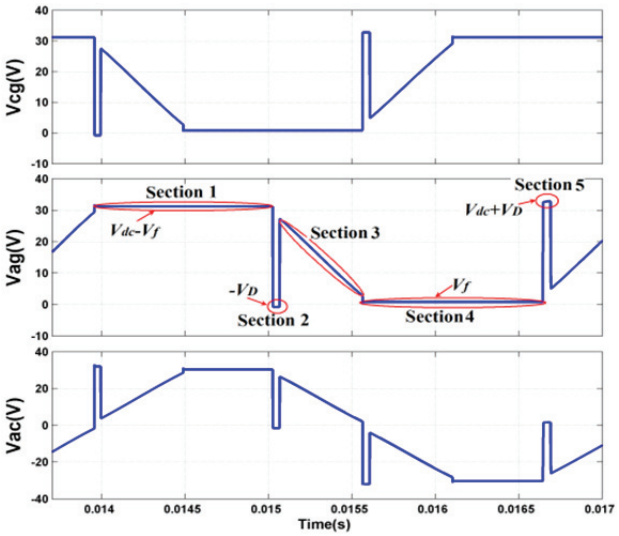

Fig. 5. Motor terminal voltages and the resultant line voltage.

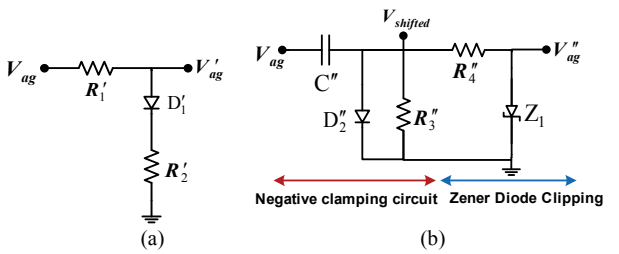

Fig. 6. Proposed sensing circuit to address the rescaling problem.

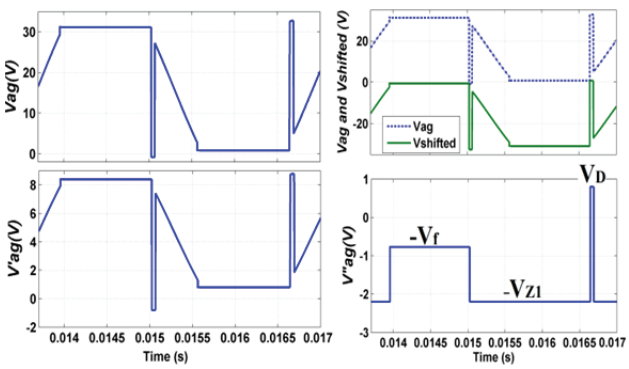

Fig. 7. (a) Voltage of phase "*a*" relative to the ground and the extracted voltage for compensating the first notch of V_{ac} . (b) Voltage V_{ag} compared to the shifted voltage $V_{shifted}$ (top) and the extracted voltage V_{ag}'' for compensating the second notch of V_{ac} (bottom).

$$V_{ag}' = \begin{cases} \left(\frac{R_2'}{R_2' + R_1'}\right)(V_{ag} - V_D) + V_D & V_{ag} > V_D \\ V_{ag} & V_{ag} \le V_D \end{cases} \quad (11)$$

where V_{ag}' is the rescaled voltage and $R_1' = 3R_2'$ (calculated for the motor of Table I). The proposed circuit rescales the input voltage if it is greater than V_D; otherwise, the input voltage will be left unchanged. In Fig. 7(a), voltage

V_{ag} is the input and V'_{ag} as is the output of the proposed sensing circuit. The figure confirms that the diode/transistor forward voltage drop is detectable compared with the peak value of the output voltage. The rescaled voltage V'_{kg} (k=a,b,c) should replace the terminal voltage in Eq. (5).

The amplitude of V_{ag} is greater than the DC-link voltage only when diode D_1 is conducting, i.e., in Section 5, which coincides with the second notch of V_{ac}. Hence, this property of V_{ag} can be used to generate an appropriate signal to compensate for the second notch of V_{ac}. Accordingly, we use a negative unbiased clamp circuit, as shown in Fig. 6(b), to shift voltage V_{ag} downwards by V_{dc}. When V_{ag} is positive, diode D''_2 conducts and capacitor C'' charges to the peak positive value of V_{ag} minus the forward voltage drop on D''_2, i.e., $(V_{dc}+V_D)-V_D=V_{dc}$. When V_{ag} is negative, diode D''_2 does not conduct. Therefore, the output voltage can be expressed as the voltage stored in C'' plus the input voltage. Accordingly, the output voltage of the clamping circuit in Fig. 6(b) can be obtained as

$$V_{shifted} = V_{ag} - V_{dc} \tag{12}$$

Voltage $V_{shifted}$ is compared with V_{ag} in Fig. 7(b). In the next step, $V_{shifted}$ is fed to a Zener diode clipping circuit (Fig. 6(b)) to limit the peak negative value of the output voltage V''_{ag} and make it applicable to a low-voltage control circuit. Moreover, by clipping voltage $V_{shifted}$ at $-V_{Z1}=-2.2\,\text{V}$, the forward voltage drop across the diode/transistor becomes more detectable compared with the peak negative value of the output voltage. Fig. 7(b) shows V''_{ag} and confirms that it is detectable at any time.

To compensate for the undesirable level changes of the sign signals of the line voltages, we define the specific sign signals for the extracted voltages V'_{kg} and V''_{kg} (k=a,b,c) as

$$\begin{aligned} D'_{ag} &= \frac{1}{2}(1-\text{sign}(V'_{ag})) \quad , \quad D''_{ag} = \frac{1}{2}(1-\text{sign}(V''_{ag})) \\ D'_{bg} &= \frac{1}{2}(1-\text{sign}(V'_{bg})) \quad , \quad D''_{bg} = \frac{1}{2}(1-\text{sign}(V''_{bg})) \\ D'_{cg} &= \frac{1}{2}(1-\text{sign}(V'_{cg})) \quad , \quad D''_{cg} = \frac{1}{2}(1-\text{sign}(V''_{cg})) \end{aligned} \tag{13}$$

Figs. 8(a) to 8(c) show the sign signals that are required to generate the VHS for phase "a". The commutation ripple that causes the first notch of D_{ac} also affects D'_{ag}. The other commutation ripple that creates the second notch of D_{ac} also influences D''_{ag}. In accordance with the arrangement of the commutation notches, a set of logical equations is defined to generate VHSs as

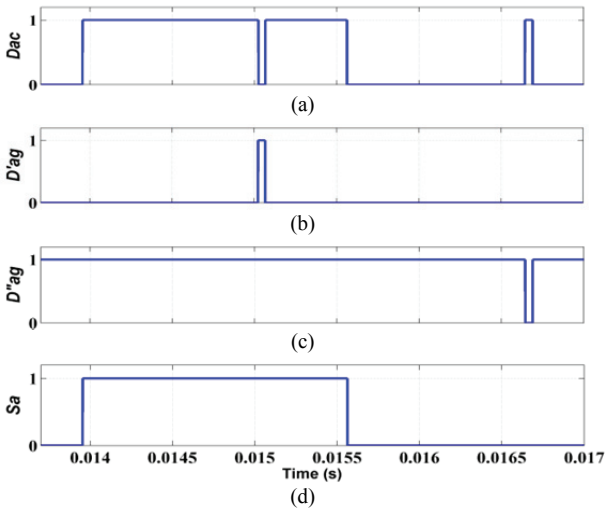

Fig. 8. From top to bottom: sign signals of the line voltage, V'_{ag}, V''_{ag}, and the extracted VHS.

$$\begin{aligned} S_a &= (D_{ac} + D'_{ag}) \bullet D''_{ag} \\ S_b &= (D_{ba} + D'_{bg}) \bullet D''_{bg} \\ S_c &= (D_{cb} + D'_{cg}) \bullet D''_{cg} \end{aligned} \tag{14}$$

where S_x ($x=a,b,c$) denotes the VHS extracted using the proposed method. The symbols $\bullet$ and $+$ represent the "AND" and "OR" operators, respectively. The extracted VHS of phase "a" is shown in Fig. 8(d).

IV. Simulation Results of the Proposed Sensorless Method

To implement the proposed method, Eq. (5), (13), and (14) are simulated in PSpice software using the three designed circuits numbered 1–3, as shown in Fig. 9. The rescaled voltages V'_{ag}, V'_{bg}, V'_{cg}, V''_{ag}, V''_{bg}, and V''_{cg} are fed to the designed circuits. In the first circuit, which is numbered "1", the rescaled voltages V'_{ag}, V'_{bg}, and V'_{cg} are fed to the subtracters to create the appropriate line voltages. Then, the line voltages are compared with the zero level by using Schmitt trigger comparators and the sign signals D_{ac}, D_{ba}, and D_{cb} are generated. Similarly, the second circuit receives the voltages V''_{ag}, V''_{bg}, and V''_{cg} and generates the sign signals D''_{ag}, D''_{bg}, and D''_{cg}. The third circuit receives the rescaled voltages V'_{ag}, V'_{bg}, and V'_{cg} and produces the sign signals D'_{ag}, D'_{bg}, and D'_{cg}. In this study, comparators with a hysteresis loop are adopted instead of conventional comparators to achieve noise-free and clean zero-crossing signals. A small hysteresis of 100 mV is integrated into the comparator to prevent the noise within the hysteresis band from crossing the threshold and producing false ZCPs. Therefore, additional noise immunity and stability can be

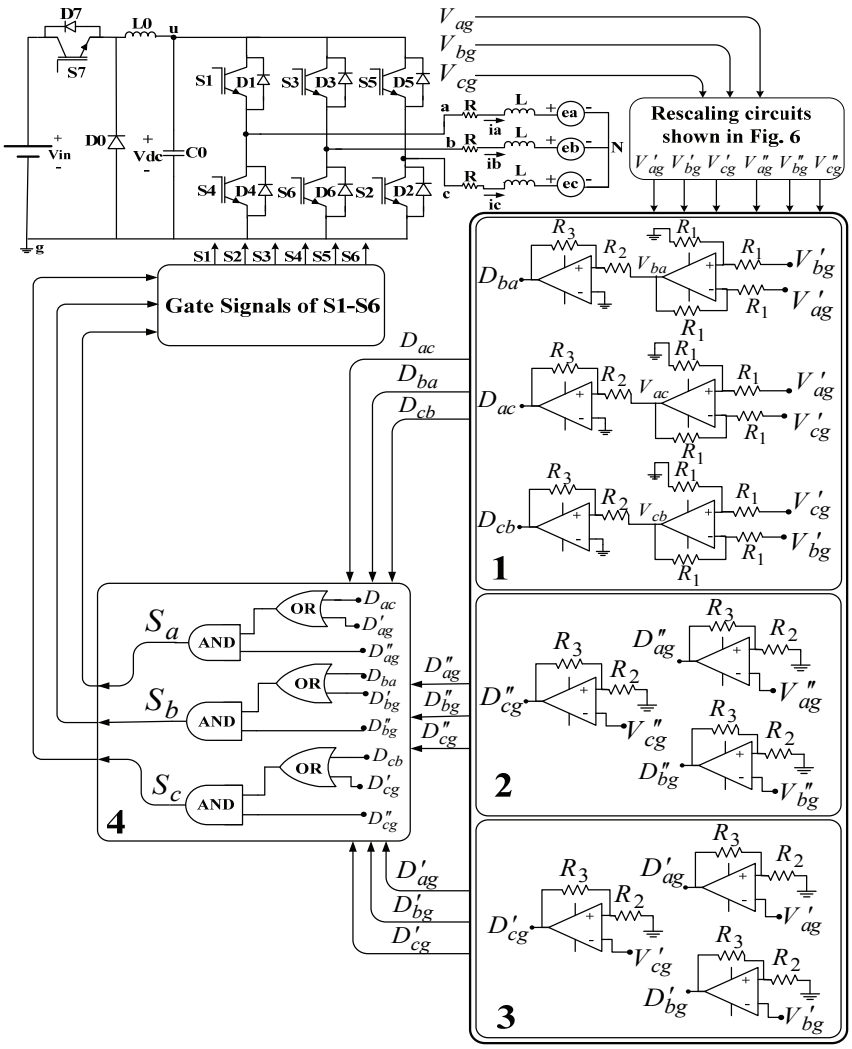

Fig. 9. Overall schematic of the proposed sensorless commutation method for BLDC motors.

obtained and the performance of the sign signal generator circuit can be improved. In accordance with Eq. (14), the sign signals are used to derive the VHSs by using circuit number 4 shown in Fig. 9.

The specifications of the EC-22-167129 Maxon motor that is used to run the simulations in MATLAB/Simulink are listed in Table I. To verify the effectiveness of the proposed method, we compare its results with those of the traditional filtered line voltage ZCP detection method. The phase delay caused by LPFs used in the traditional method depends on their cutoff frequency. Hence, to improve comparison, Fig. 10 shows the simulated phase delay of LPFs with different cutoff frequencies at varying rotor speed values. A low cutoff frequency leads to a considerable phase delay. By contrast, an LPF with a high cutoff frequency cannot completely eliminate switching and commutation noise. Consequently, a trade-off is required between LPF phase delay and noise elimination. In this study, the cutoff frequency of 2 kHz is selected for the LPFs used in the traditional method.

TABLE I
SPECIFICATIONS OF THE EC-22-167129 MAXON MOTOR

Parameter	Value
Rated power	50 W
Speed constant	702 rpm/V
Torque constant	13.6×10^{-3} Nm/A
Pole pairs	1
Rated voltage	32 V
Rotor inertia	4.2×10^{-7} kg.m^2
Stator resistance	0.4985 Ω
Stator inductance	0.0735 mH
Rated speed	20200 rpm
Voltage constant	13.6×10^{-3} V/rad/s

The line voltage, phase current, electromagnetic torque, and rotor speed obtained from the proposed and traditional methods are shown in Figs. 11 and 12, respectively. In Figs. 11(d) and 12(d), the IHS (H_a) is compared with the VHS (S_a) extracted using the proposed and traditional methods.

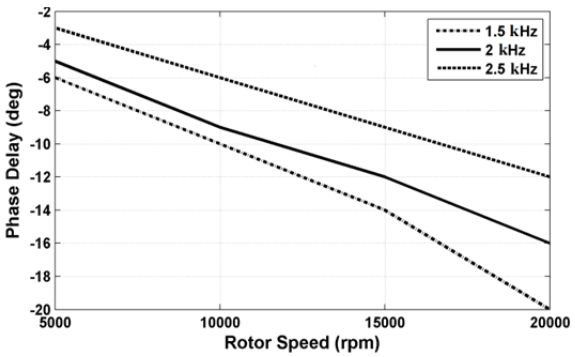

Fig. 10. Comparison of the simulated phase delay vs. the rotor speed caused by LPFs with different cutoff frequencies.

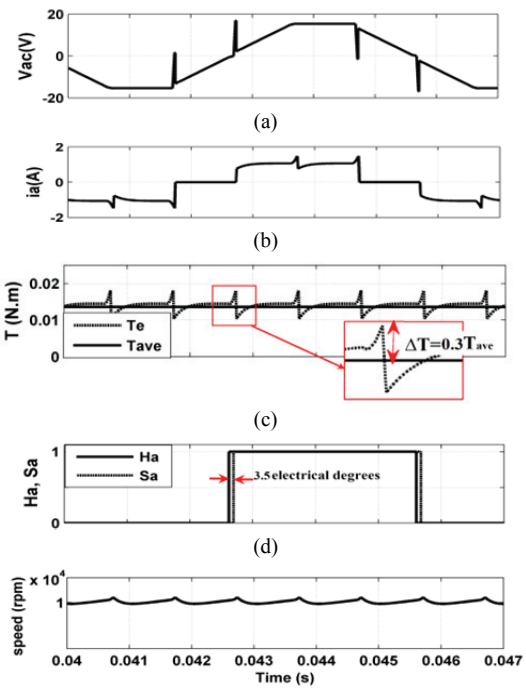

Fig. 11. Simulated waveforms of the proposed method under an intermediate load at a speed of 10000 rpm: (a) Line voltage, (b) Phase current, (c) Electromagnetic torque, (d) IHS and VHS, (e) Rotor speed.

The simulation results are presented under an intermediate load at a speed of 10000 rpm. The VHS obtained using the proposed method clearly exhibits good agreement with the IHS. The commutation angle error is approximately 3.5° for the proposed method, whereas it is significant and approximately 11° for the traditional method. The slight difference between the IHS and the proposed VHSs is due to the voltage drop on the stator resistance. The current and torque distortion are determined to be smaller when the proposed method is used by comparing the electromagnetic torque and phase current waveforms of the proposed and traditional methods. The peak-to-peak values of the phase current are 3 A and 4 A for the proposed and traditional methods, respectively. Furthermore, the torque ripple is 30%

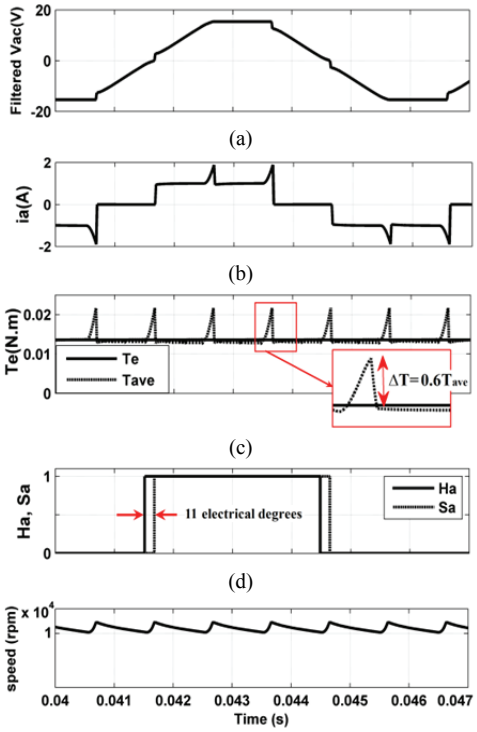

Fig. 12. Simulated waveforms of the traditional method under an intermediate load at a speed of 10000 rpm: (a) Line voltage, (b) Phase current, (c) Electromagnetic torque, (d) IHS and VHS, (e) Rotor speed.

and 60% of the average torque for the proposed and traditional methods, respectively. Therefore, the rotor speed of the proposed method produces smaller ripples than the traditional method as shown in Figs. 11(e) and 12(e).

Another simulation is conducted under an intermediate load at a speed of 15000 rpm. The results of the proposed and traditional methods are shown in Figs. 13 and 14, respectively. The commutation angle error for the proposed method is approximately 3°, whereas that for the traditional method is significant and approximately 14°. The torque ripple is approximately 33% and 83% of the average torque for the proposed and traditional methods, respectively. The peak-to-peak value of the phase current is 3 A and 5 A for the proposed and traditional methods, respectively. The current ripple produced by the proposed method is smaller than that produced by the traditional method. Evidently, the larger the position error, the larger the rotor speed ripple, as shown in Figs. 13(e) and 14(e).

We repeat the simulation at different rotor speeds to compare the position error of the proposed method with that of the traditional method. Fig. 15 shows the simulated performance of the proposed and traditional methods at different speeds. Evidently, the commutation angle error of the traditional method increases with an increase in rotor speed. Consequently, the traditional method is unsuitable for a wide range of speed. By contrast, increasing or decreasing

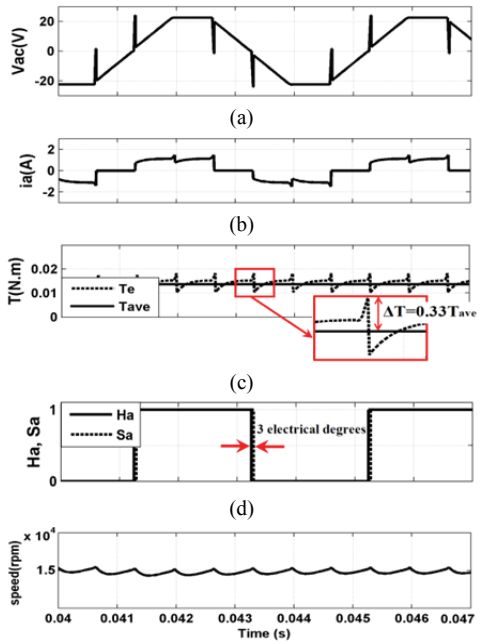

Fig. 13. Simulated waveforms of the proposed method under an intermediate load at a speed of 15000 rpm: (a) Line voltage, (b) Phase current, (c) Electromagnetic torque, (d) IHS and VHS, (e) Rotor speed.

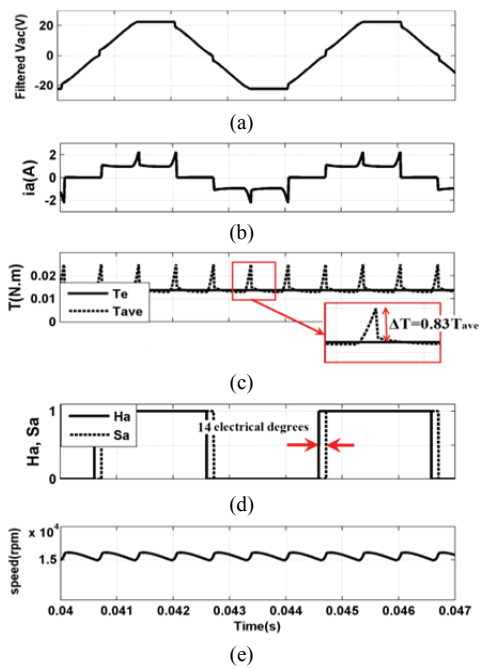

Fig. 14. Simulated waveforms of the traditional method under an intermediate load at a speed of 15000 rpm: (a) Line voltage, (b) Phase current, (c) Electromagnetic torque, (d) IHS and VHS, (e) Rotor speed.

rotor speed does not significantly affect the performance of the proposed method.

Fig. 16 shows the phase delays of the proposed and traditional methods vs. the load torque at a speed of 20000 rpm. The negligible phase delay of the proposed method originates from the voltage drop on the stator resistance. The phase delay is zero under no-load condition for the proposed method. By contrast, the traditional method exhibits a remarkable phase delay even under no-load condition.

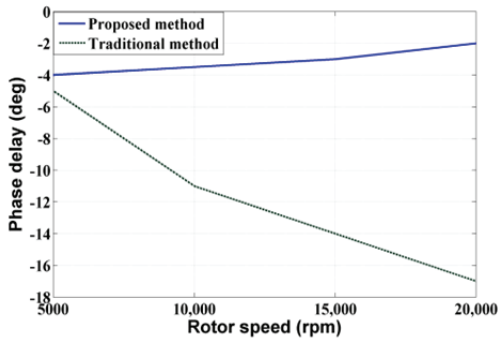

Fig. 15. Comparison of the simulated phase delay vs. rotor speed for the proposed and traditional methods.

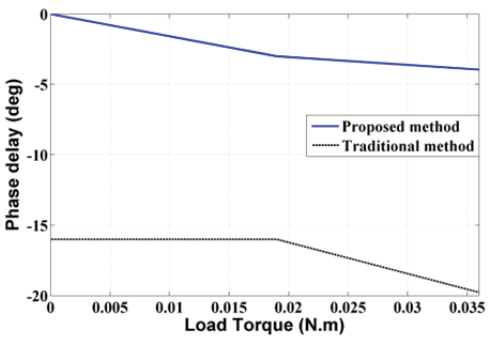

Fig. 16. Comparison of the simulated phase delay vs. load torque at a speed of 20000 rpm for the proposed and traditional methods.

V. Experimental Results

The experimental setup (Fig. 17) includes a Maxon BLDC motor with the specifications listed in TABLE I, a DC generator (used as the load), a digital oscilloscope, the designed circuits (for the proposed sensorless operation), and a three-leg inverter. Moreover, a Lutron DT-2236C digital tachometer is used to measure rotor speed. Phase currents are measured by using very small resistors connected in series to motor phases. The required voltages are generated by the circuits shown in Fig. 6. The experimental waveforms of the voltages V_{ag}, V'_{ag}, $V_{shifted}$, and V''_{ag} extracted from the proposed circuits are illustrated in Fig. 18. They justify the capability of the proposed sensing circuits to properly generate compensator signals. Fig. 19 shows the experimental waveforms of the voltages V_{ac}, V'_{ag}, and V''_{ag}, along with their sign signals.

The experimental waveforms of the line voltage, phase current, motor speed, electromagnetic torque, IHS produced by the Hall sensors placed within the motor, and VHS extracted

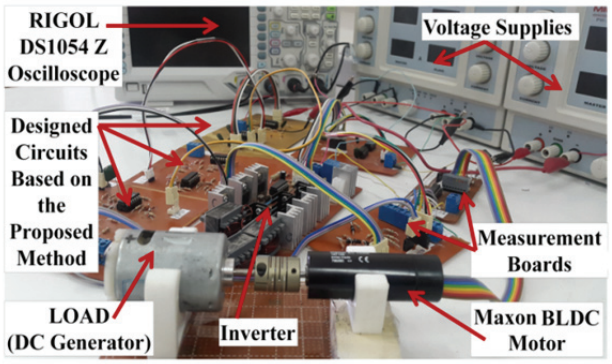

Fig. 17. Experimental setup of the proposed sensorless commutation method.

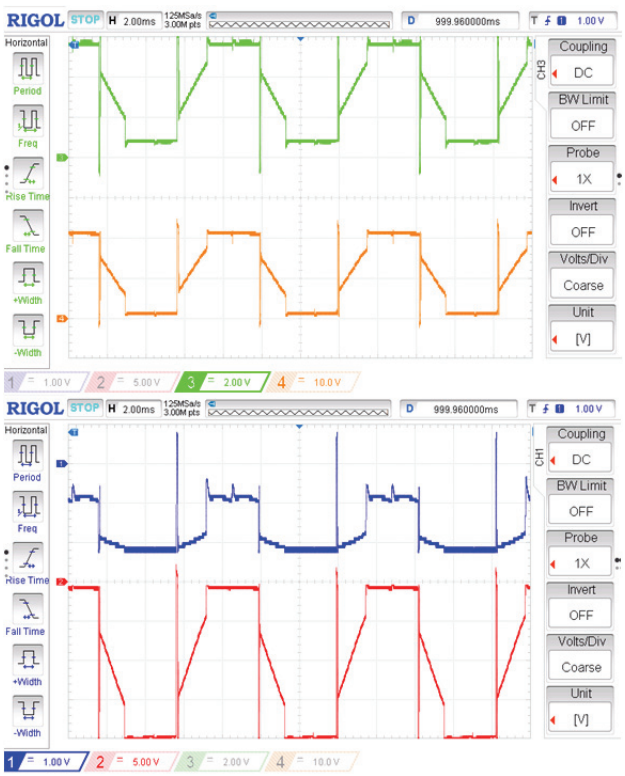

Fig. 18. From top to bottom: experimental waveforms of V'_{ag} (2 V/div), V_{ag} (10 V/div), V''_{ag} (1 V/div), and $V_{shifted}$ (5 V/div).

using the proposed and traditional methods at a speed of 10000 rpm are shown in Figs. 20 and 21, respectively. The position errors from the proposed and traditional methods are 4° and 13°, respectively. The peak-to- peak values of the phase current are approximately 2.5 A and 4 A for the proposed and traditional methods, respectively. The position error of the proposed method is smaller than that of the traditional method. Consequently, the current ripple of the proposed method is less than that of the traditional method. Furthermore, the ripples of speed and torque are smaller in the proposed method compared with those in the traditional method.

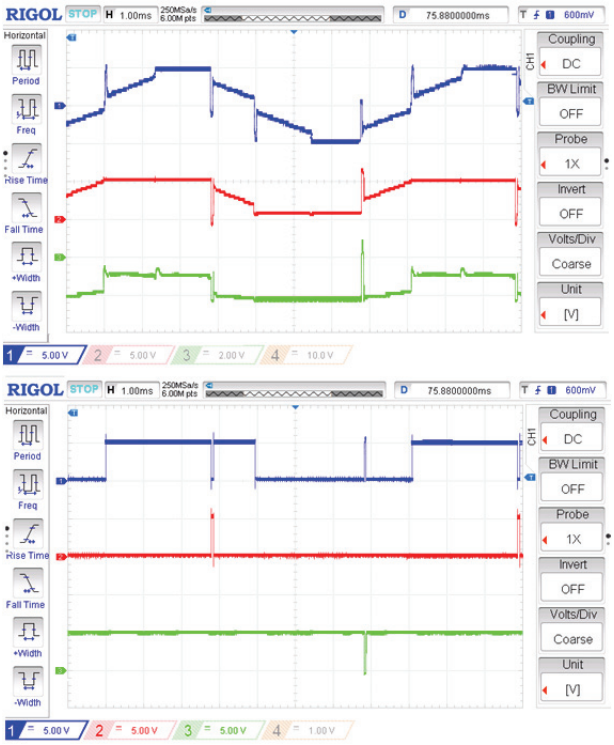

Fig. 19. From top to bottom: Experimental waveforms of V_{ac} (5 V/div), V'_{ag} (5 V/div), V''_{ag} (2 V/div), D_{ac}, D'_{ag}, and D''_{ag}.

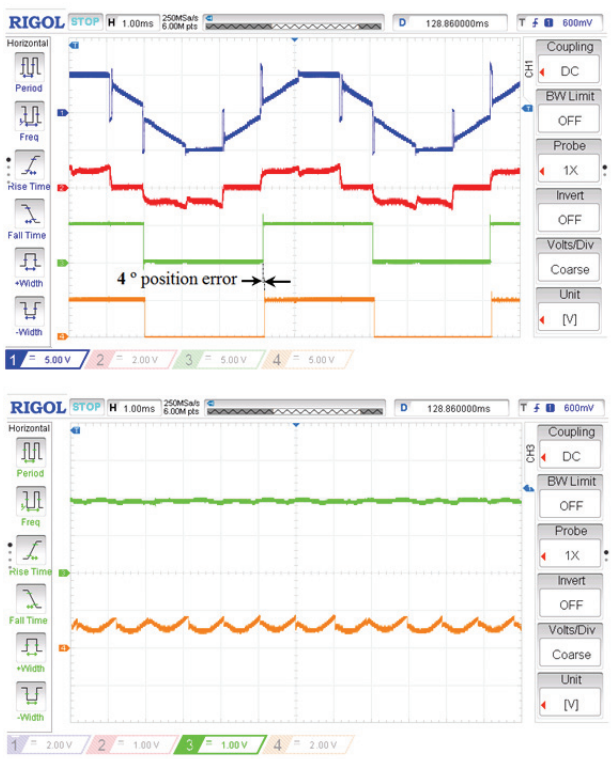

Fig. 20. Experimental waveforms obtained using the proposed method at a speed of 10000 rpm (from top to bottom): line voltage (5 V/div), phase current (2 A/div), IHS, VHS, rotor speed (5000 rpm/div), and electromagnetic torque (0.02 N.m/div).

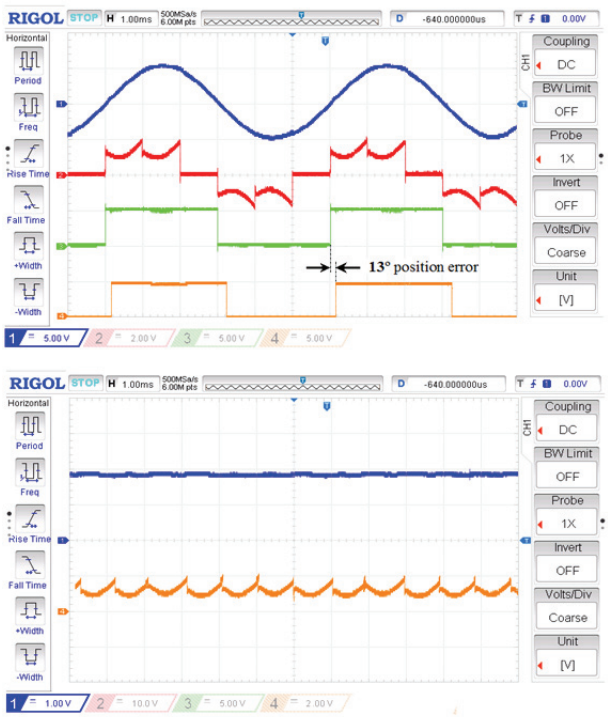

Fig. 21. Experimental waveforms obtained using the traditional method at a speed of 10000 rpm (from top to bottom): line voltage (5 V/div), phase current (2 A/div), IHS, VHS, rotor speed (5000 rpm/div), and electromagnetic torque (0.02 N.m/div).

Fig. 22. Experimental waveforms obtained using the proposed method at a speed of 15000 rpm (from top to bottom): line voltage (5 V/div), phase current (2 A/div), IHS, and VHS.

The experimental results of the proposed and traditional methods at a speed of 15000 rpm are shown in Figs. 22 and 23, respectively. The position errors from the proposed and traditional methods are 4° and 16°, respectively. The position error from the traditional method increases with an increase in rotor speed.

To test the dynamic performance of the proposed method, motor speed is suddenly changed from 3000 rpm to 15000 rpm. The waveforms of rotor speed, V_{ac} and i_a, are shown in Fig. 24. They verify the good performance of the proposed method when the speed of the motor suddenly changes.

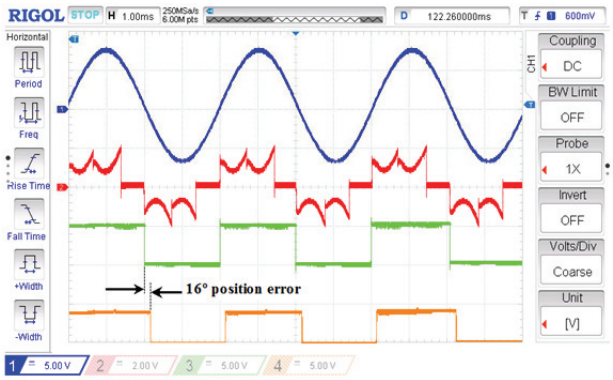

Fig. 23. Experimental waveforms obtained using the traditional method at a speed of 15000 rpm (from top to bottom): line voltage (5 V/div), phase current (2 A/div), IHS, and VHS.

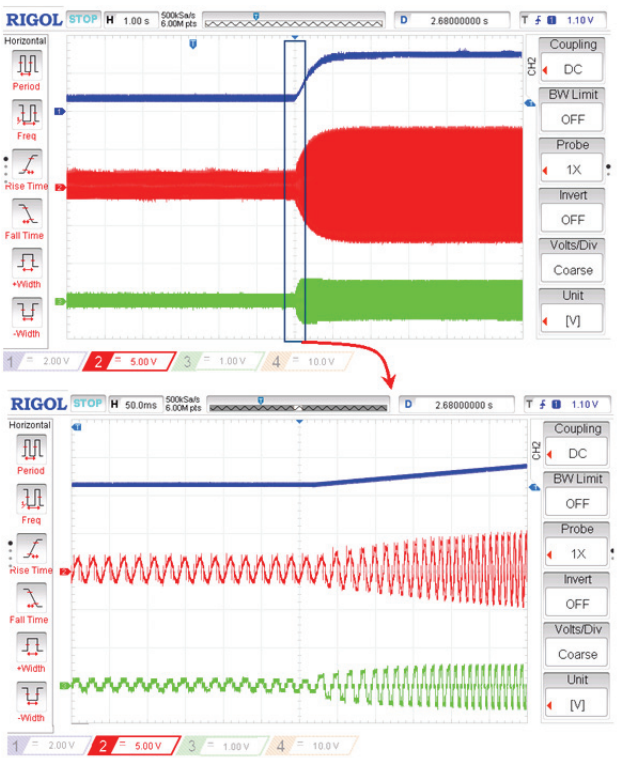

Fig. 24. From top to bottom: experimental waveforms of rotor speed (CH1: 10000 rpm/div), line voltage (CH2: 5 V/div), and current (CH3: 2 A/div) during a sudden change in rotor speed.

TABLE II
COMPARISON OF THE SPECIAL FEATURES IN [16]–[22] AND THE PROPOSED METHOD

Special Features	[16]–[19]	[20]	[21]	[22]	Proposed Method
Number of Voltage Sensors	3	3	1	4	3
Current Sensor	×	×	√	×	×
Neutral Point	×	×	√	√	×
Phase Shifter	×	√	√	×	×
LPF	√	√	√	√	×

× = Not required, √ = required

VI. CONCLUSIONS

A new sensorless commutation method for BLDC motors is introduced in this study. The proposed method uses unfiltered line voltages. Specific voltage sensing circuits are proposed to generate the appropriate compensator signals. Then, virtual Hall signals are derived by applying a set of proposed logical operations to the sign signals. Compared with the previous methods, the proposed method increases motor speed range by eliminating LPFs. Moreover, this method is less complicated due to the absence of a phase shifter. The proposed approach can be easily implemented using simple comparators without requiring high-cost DSP. The position error and torque ripple of the proposed method are smaller than those of traditional methods. The performance of the proposed method is insensitive to operating speed and load conditions. The simulation and experimental results prove the effectiveness of the proposed method, which is simple and cost-effective. Hence, this method can be implemented in integrated circuits for mass production. The comparison of some features of the proposed method and the methods presented in [16]–[22] is summarized in Table II.

REFERENCES

[1] Y. Xu, Y. Wei, B. Wang, and J. Zou, "A novel inverter topology for brushless DC motor drive to shorten commutation time," *IEEE Trans. Ind. Electron.,* Vol. 63, No. 2, pp. 796-807, Feb. 2016.

[2] H. Zhaobin, Y. Linru, and W. Zhaodong, "Sensorless initial rotor position identification for non-salient permanent magnet synchronous motors based on dynamic reluctance difference," *IET Power Electron.,* Vol. 7, No. 9, pp. 2336-2346, Sep. 2014.

[3] S. S. Bharatkar, R. Yanamshetti, D. Chatterjee, and A. K. Ganguli, "Dual-mode switching technique for reduction of commutation torque ripple of brushless dc motor," *IET Electric Power Appl.,* Vol. 5, No. 1, pp. 193-202, Jan. 2011.

[4] A. C. Lee, C. J. Fan, and G. H. Chen, "Current integral method for fine commutation tuning of sensorless brushless DC motor," *IEEE Trans. Power Electron.,* Vol. 32, No. 12, pp. 9249-9266, Dec. 2017.

[5] G. Haines and N. Ertugrul, "Wide speed range sensorless operation of brushless permanent-magnet motor using flux linkage increment," *IEEE Trans. Ind. Electron.,* Vol. 63, No. 7, pp. 4052-4060, Jul. 2016.

[6] A. C. Lee, S. Wang, and C. J. Fan, "A current index approach to compensate commutation phase error for sensorless brushless DC motors with nonideal back EMF," *IEEE Transa. Power Electron.,* Vol. 31, No. 6, pp. 4389-4399, Jun. 2016.

[7] K. Iizuka, H. Uzuhashi, M. Kano, T. Endo, and K. Mohri, "Microcomputer control for sensorless brushless motor," *IEEE Trans. Ind. Appl.,* Vol. IA-21, No. 3, pp. 595-601, May 1985.

[8] C. Xia, Y. Xiao, W. Chen, and T. Shi, "Torque ripple reduction in brushless DC drives based on reference current optimization using integral variable structure control," *IEEE Trans. Ind. Electron.,* Vol. 61, No. 2, pp. 738-752, Feb. 2014.

[9] S. Jianwen, D. Nolan, M. Teissier, and D. Swanson, "A novel microcontroller-based sensorless brushless DC (BLDC) motor drive for automotive fuel pumps," *IEEE Trans. Ind. Appl.,* Vol. 39, No. 6, pp. 1734-1740, Nov. 2003.

[10] S. Jianwen, "An improved microcontroller-based sensorless brushless DC (BLDC) motor drive for automotive applications," *IEEE Trans. Ind. Appl.,* Vol. 42, No. 5, pp. 1216-1221, Sep./Oct. 2006.

[11] P. Damodharan and K. Vasudevan, "Sensorless brushless DC motor drive based on the zero-crossing detection of back electromotive force (EMF) from the line voltage difference," *IEEE Trans. Energy Convers.,* Vol. 25, No. 3, pp. 661-668, Sep. 2010.

[12] P. Damodharan, R. Sandeep, and K. Vasudevan, "Simple position sensorless starting method for brushless DC motor," *IET Electric Power Appl.,* Vol. 2, No. 1, pp. 49-55, Jan. 2008.

[13] X. Z. Zhang and Y. N. Wang, "A novel position-sensorless control method for brushless DC motors," *Energy Convers. Manag.,* Vol. 52, No. 3, pp. 1669-1676, Mar. 2011.

[14] X. Changliang and L. Xinmin, "Z-source inverter-based approach to the zero-crossing point detection of back EMF for sensorless brushless DC motor," *IEEE Trans. Power Electron.,* Vol. 30, No. 3, pp. 1488-1498, Mar. 2015.

[15] J. Quan, B. Chao, and R. Huang, "A new phase-delay-free method to detect back EMF zero-crossing points for sensorless control of spindle motors," *IEEE Trans. Magn.,* Vol. 41, No. 7, pp. 2287-2294, Jul. 2005.

[16] T. Y. Kim and J. Lyou, "Commutation instant detector for sensorless drive of BLDC motor," *Electron. Lett.,* Vol. 47, No. 23, pp. 1269-1270, Nov. 2011.

[17] S. Mahdiuon-Rad, M. R. Azizian, and S. Soleimanpour, "Modeling, simulation and implementation of a sensorless commutation method for brushless DC motors without phase shifter," in *Power Electronics, Drives Systems & Technologies Conference (PEDSTC), 2015 6th*, pp. 228-233, 2015.

[18] C. Cheng-Hu and C. Ming-Yang, "A new cost effective sensorless commutation method for brushless DC motors without phase shift circuit and neutral voltage," *IEEE Trans. Power Electron.,* Vol. 22, No. 2, pp. 644-653, Mar. 2007.

[19] T.-W. Chun, Q.-V. Tran, H.-H. Lee, and H.-G. Kim, "Sensorless control of BLDC motor drive for an automotive fuel pump using a hysteresis comparator," *IEEE Trans. Power Electron.,* Vol. 29, No. 3, pp. 1382-1391, Mar. 2014.

[20] G. Liu, C. Cui, K. Wang, B. Han, and S. Zheng, "Sensorless control for high-speed brushless DC motor based on the line-to-line back EMF," *IEEE Trans. Power Electron.,* Vol. 31, No. 7, pp. 4669-4683, Jul. 2016.

[21] C. Chenjun, L. Gang, W. Kun, and S. Xinda, "Sensorless drive for high-speed brushless DC motor based on the virtual neutral voltage," *IEEE Trans. Power Electron.,* Vol. 30, No. 6, pp. 3275-3285, Jun. 2015.

[22] W. Li, J. Fang, H. Li, and J. Tang, "Position sensorless control without phase shifter for high-speed BLDC motors with low inductance and nonideal back EMF," *IEEE Trans. Power Electron.,* Vol. 31, No. 2, pp. 1354-1366, Feb. 2016.

[23] A. Halvaei Niasar, A. Vahedi, and H. Moghbelli, "Low-

cost sensorless control of four-switch, brushless DC motor drive with direct back-EMF detection," *J. Zhejiang Univ. Science A,* Vol. 10, No. 2, pp. 201-208, Feb. 2009.

[24] A. H. Niasar, H. Moghbelli, and A. Vahedi, "A low-cost sensorless control for reduced-parts, brushless DC motor drives," in *Industrial Electronics, ISIE 2008. IEEE International Symposium on*, pp. 662-667, 2008.

[25] A. Halvaei Niasar, A. Vahedi, and H. Moghbelli, "A novel position sensorless control of a four-switch, brushless DC motor drive without phase shifter," *IEEE Trans. Power Electron.,* Vol. 23, No. 6, pp. 3079-3087, Nov. 2008.

[26] F. Jiancheng, L. Wenzhuo, and L. Haitao, "Self-compensation of the commutation angle based on DC-link current for high-speed brushless DC motors with low inductance," *IEEE Trans. Power Electron.,* Vol. 29, No. 1, pp. 428-439, Jan. 2014.

[27] F. Jiancheng, Z. Xinxiu, and L. Gang, "Instantaneous torque control of small inductance brushless DC motor," *IEEE Trans. Power Electron.,* Vol. 27, No. 12, pp. 4952-4964, Dec. 2012.

[28] S. Iwasaki, R. P. Deodhar, L. Yong, A. Pride, Z. Q. Zhu, and J. J. Bremner, "Influence of PWM on the proximity loss in permanent-magnet brushless AC machines," *IEEE Trans. Ind. Appl.,,* Vol. 45, No. 4, pp. 1359-1367, Jul./Aug. 2009.

[29] F. Jiancheng, Z. Xinxiu, and L. Gang, "Precise accelerated torque control for small inductance brushless DC motor," *IEEE Trans. Power Electron.,* Vol. 28, No. 3, pp. 1400-1412, Mar. 2013.

[30] F. Jiancheng, L. Haitao, and H. Bangcheng, "Torque ripple reduction in BLDC torque motor with nonideal back EMF," *IEEE Trans. Power Electron.,* Vol. 27, No. 11, pp. 4630-4637, Nov. 2012.

[31] K.-H Kim and M.-J. Yoon, "Performance comparison of PWM inverter and variable DC link inverter schemes for high-speed sensorless control of BLDC motor," *Electron. Lett.,* Vol. 38, No. 21, pp. 1294-1295, Oct. 2002.

Shahin Mahdiyoun Rad obtained her B.Sc. in Electronics Engineering from the University of Zanjan, Iran, in 2008, and her M.Sc. in Electrical Engineering from the University of Tabriz, Iran, in 2011. She is currently working toward her Ph.D. in the Department of Electrical Engineering, Sahand University of Technology, Tabriz, Iran. Her current research interests include control of electrical drives and electrical machines.

Mohammad Reza Azizian obtained his B.Sc. and M.Sc. from the University of Tabriz, Tabriz, Iran, in 1988 and 1991, respectively, and his Ph.D. from Brno University of Technology, Brno, Czech Republic, in 2003, all of which in Electrical Engineering. From 1991 to 1999, he worked as a research assistant at the Department of Electrical Engineering in Sahand University of Technology, Tabriz, Iran, where he is currently a faculty member and an associate professor. He teaches electrical drives and power electronics courses. His research interests include sensorless control of electrical drives and the design and implementation of power converters.